Characterisation of iron (II) sulfides in wet archaeological woods: the wreck of Mandirac (IV th century, antique ports of Narbonne, France)

Céline Remazeilles, Francois Leveque, Maylis Minjacq, Philippe Refait, Corinne Sanchez, Marie-Pierre Jézégou

Characterisation of iron (II) sulfides in wet archaeological woods: the wreck of Mandirac (IVth century, antique ports of Narbonne, France)

Céline Rémazeilles[a*], François Lévêque[b], Maylis Minjacq[ab], Philippe Refait[a], Corinne Sanchez[c], Marie-Pierre Jézégou[d]

[a]LaSIE, Laboratory of Engineering Sciences for the Environment
UMR 7356 CNRS/University of La Rochelle
cremazei@univ-lr.fr

[b]LIENSs, Littoral, Environment and Societies
UMR 7266 CNRS/University of La Rochelle

[c]ASM, Archaeology of Mediterranean Societies
UMR-5140 CNRS/University of Montpellier
Ministry of Culture and Communication/INRAP, French National Institute for Preventive Archaeological Research

[d]DRASSM, Department for Underwater and Undersea Archaeological Research

Abstract
The wreck of Mandirac (Narbonne, France, IV century) was excavated in 2013 and 2014 from waterlogged soil. A magnetic prospection campaign performed in 2014 revealed that the wood was abnormally magnetic. A plank extracted from the hull, containing an iron nail, was analysed using Environmental Scanning Electron Microscopy, micro-Raman spectroscopy, X-Ray diffraction and magnetic characterization methods in order to identify the mineral composition inside the wood and of the nail. Results revealed an accumulation of greigite and pyrite in the wood around the nail, where the pH was measured below 3. The nail was completely corroded into pyrite and siderite, with no metal left. Marcasite was also identified far from the nail, where the pH was measured around 5. Greigite was the only phase responsible of the magnetic signal emitted from the wood and proved to be present in varying amounts throughout the entire wreck. The iron sulfides were probably formed via anaerobic sulphidogenic bacteria influenced corrosion processes, which occurred on the nails. These results are very different from those obtained from more recent shipwrecks (XIX century). So the nature of these iron sulfides in wet archaeological woods is discussed.

Keywords
Waterlogged soil, archaeological wood, microbiologically influenced corrosion, iron sulfides, greigite, pyrite, Mandirac.

Introduction
Waterlogged archaeological wood contaminated by iron and extracted from biologically active and anoxic environments are exposed to dramatic post-excavation damage. During the burial, sulfides generating bacteria can reduce oxygenated compounds of sulfur (sulphates, sulphites, etc), present in the environment, into sulfide species (H_2S, HS^-, S^{2-}). These latter, combined with iron (II) ions resulting from the corrosion of iron objects used for assembly, can precipitate into iron (II) sulfides. The chemistry of iron (II) sulfides is complex and implies anoxic (on-site) transformations as well as transformations controlled by oxygen (once exposed to air). Post-excavation damage observed on wood is mainly caused by the precipitation of voluminous crystals and acidification leading to the formation of cracks and crumbs, unsightly

efflorescence, decay of the organic matter and loss of mechanical strength. Iron and/or sulfur-containing phases proved to have a strong influence in the degradation mechanisms (Sandström et al. 2002, Fors and Sandström 2006). Pyrite (FeS_2) and mineral sulfur (α-S_8) are often mentioned in wet archaeological woods but mackinawite (FeS) and greigite (Fe_3S_4) were also detected in significant amounts (Rémazeilles et al. 2013).

This paper deals with the identification of iron/sulfur-containing phases present in a plank of wood containing the remains of an iron nail. The plank was extracted from a IV century wreck, discovered in waterlogged soil during excavations of the ancient ports of Narbonne (Castélou/Mandirac - Mediterranean coast, France). The site is now inland. A magnetic prospection campaign performed on site in 2014 revealed that the wood of the entire wreck was abnormally magnetic. It also determined that there was no metal left in the nails used for assembly. Consequently, the magnetic signal was supposed to come from the diffusion of magnetic corrosion products inside the wooden planks. Several iron-containing compounds like magnetite (Fe_3O_4), maghemite (γ-Fe_2O_3), greigite (Fe_3S_4) and pyrrhotite ($Fe_{(1-x)}S$) and smithyte (Fe_9S_{11}) are naturally magnetic. The possible presence of iron sulfides would imply conservation concerns for this wreck. Actually pyrite (FeS_2) was visually observed in the vicinity of 'ghost' iron nails. A study was then carried out in order to identify the mineral phases present in the wood and to be able to attribute the magnetic signal to one or several of the compounds.

The chemistry of iron sulfides has been widely studied. Their occurrence is mostly explained by microbiological activity and mackinawite is considered as the first precipitate from which arise several mechanisms of transformation. Parameters like the oxic/anoxic feature of the environment, sulfur supply via sulfide species production, temperature, humidity, pH, etc, determine one pathway or another. The diagram in Figure 1 summarises the oxidation processes of mackinawite according to different pathways proposed in literature (Hunger and Benning 2007, Bourdoiseau et al. 2008, Bourdoiseau et al. 2011, Rickard and Luther 1997, Wilkin and Barnes 1997). Once exposed to air, mackinawite is transformed into mineral sulfur (α-S_8) and iron oxyhydroxides via greigite. Under anoxic conditions and with a sufficient sulfur supply, mackinawite leads to pyrite via greigite.

The subsequent oxidation of pyrite has also been largely studied (Hunger and Benning 2007, Bourdoiseau et al. 2008, Garrels and Thompson 1960, Stumm and Morgan 1981, Sullivan et al. 1988). Mechanisms proposed in literature lead to the formation of Fe(II) sulphates and to sulfuric acid (Figure 1). Wet archaeological wood contaminated by iron is seriously affected by such phenomena. The concomitant presence of abundant organic matter and a corroding iron object is a particularly fertile ground for the development of anaerobic sulfides generating bacteria colonies and iron sulfide production. Mackinawite, greigite, pyrite and marcassite have already been found in wood samples extracted from wrecks (Rémazeilles et al. 2013). However there are other naturally occurring iron sulfides, as reported in Table 1. To the best of our knowledge troilite, pyrrhotite and smythite were never clearly identified in archaeological wood. As pyrrhotite and smythite present characteristic magnetic properties, magnetic characterisation methods, much more sensitive than conventional methods, would help to detect them even in very small amounts.

The present paper deals with the analytic results obtained by a combination of characterisation methods like remanent magnetisation measurements, micro-Raman spectroscopy, X-Ray Diffraction (XRD), Environmental Scanning Electron Microscopy coupled to Energy Dispersive Spectroscopy (ESEM-EDS). Another aim of the study was to assess the potential of

magnetic characterisation methods for the detection of some iron sulfides and their suitability for non-destructive analysis. Finally, the nature of expected iron sulfides in wet archaeological wood will be discussed.

Materials and methods

Archaeological and scientific contexts

Ancient ports of Narbonne have been excavated since 2010 but the site was discovered in 1945 from aerial photographs. In 2007 a geophysics multi-methods survey confirmed the presence of the remains of infrastructures of fluvio-lagoonal harbour systems. A channelled river was identified with the dikes covered by more recent deposits of the floodplain. So a research program was launched in 2010 and several merchandise unloading zones were localised. During the excavation of one site (Castélou/Mandirac), the remains of a boat with its load of amphorae had been detected in a segment of the dike (Figure 2) (Sanchez and Jézégou 2014). The boat was actually deliberately sunk during the IV century in order to consolidate the dike. Several planks were recovered from the wreck for analysis and the results presented in this paper were obtained on the plank, *vaigre 11* (Figure 3). This plank is about 80 cm long, 16.5 cm wide and 2.5 cm thick.

Sampling

In order to preserve oxygen sensitive compounds, the planks were wrapped in a plastic film after recovery and frozen at -4°C at the laboratory until analysis. The study of *vaigre 11* was performed using a combination of complementary techniques. *Vaigre 11* was firstly gridded in rows and columns and a magnetic susceptibility mapping (SM-30 shirt pocket-size magnetic susceptibility meter, ZH instruments) was carried out (Figure 3). Then the plank was cut into 2 x 2 x 2 cm^3 cubes with a circular saw equipped with a Teflon blade. Twelve squares are represented on the plank, superimposed on the magnetic susceptibility mapping (Figure 3) and correspond to the samples that were analysed. These samples were chosen along line e and column 20 extending from the most magnetic point at position e20. The sample cubes were named according to their grid position on the plank.

A ‘ghost’ nail was evident inside cube g20. This was extracted, embedded in epoxy resin and cut with a diamond wire saw in order to perform analysis on the cross section. The section was ground with SiC papers using hexane and polished with a 3 μm diamond water free paste (DP-Suspension A, Struers).

Analytical methods

Magnetic measurements were realized in a first time, directly on the cubes. Low field magnetic susceptibility was measured with a KLY4 – Agico. First acquisition and backfield demagnetization of isothermal remanent magnetisation (IRM) were acquired up to 3T with a MMPM10 Magnetic Measurements pulse magnetizer and measured with a JR6 Agico spinner magnetometer. The magnetic susceptibility presents a wide range of variation over three orders of magnitude from negative to strong positive values. An arbitrary constant of 25 10^{-6} is added in order to proceed to a $\log_{10}$ transform. This allows only the para- and ferro-magnetic *s.l.* components to be observed, removing the diamagnetic ones (i.e. wood and the water content).

Then, optical microscopy, ESEM-EDS, micro-Raman spectroscopy and XRD were applied on slices cut from each cube. It is important to precise that the experiments were performed without any special protection against air. Metastable iron sulfides tend to transform once exposed to oxygen, therefore a slice was cut from the surface of each cube with a scalpel immediately before the use of each technique so that always a freshly cut surface was analysed.

A preliminary examination was performed with a stereomicroscope (Leica, M165C) for macroscopic observations.

Micro-Raman spectroscopy (μ-RS) experiments were performed with a Jobin Yvon High Resolution spectrometer (LabRAM HR) equipped with a microscope and a Peltier-based cooled charge coupled device detector. The laser power was filtered to avoid transformation of the sample by heating and spectra were recorded at a resolution of 0.2 cm^{-1}. Samples were studied with an excitation wavelength of 632.82 nm.

High-resolution micrographs and elemental compositions were obtained with a SEM-FEI, Quanta 200 FEG/ESEM coupled with an X-ray microanalysis EDS EDAX Genesis system. Observations were performed in low-pressure gaseous environment (0.002 atm), high relative humidity and with an acceleration voltage between 15 and 20 kV. This experimental mode does not require any preparation of non-conducting samples and the wood slices were placed wet in the analytic chamber.

XRD analyses were performed with an INEL EQUINOX 6000 diffractometer, using Co-Kα wavelength (λ = 0.17903 nm). A freshly cut slice was placed directly on the sample holder and exposed to the x-ray beam. The diffraction patterns were processed with the EVA software and the ICDD-JCPDS database.

In addition, pH measurements were performed on another freshly cut surface of each cube (Sentix Sur WTW, electrode designed for surface measurements).

μ-RS, ESEM-EDS and XRD are considered herein as "conventional methods", with respect to magnetic methods, not usually used in this context.

Results

Identification of mineral phases inside the wood

Results are summarized in Table 2 but as representative examples, only samples e4, e14, e20 and h20 are described in detail. The remanent hysteresis curves are very similar (Figure 3) and characteristic of greigite, with grain sizes of about 20-500 nm (Roberts et al. 2011). The greigite content, which was extrapolated from theoretical remanent saturation magnetization (Ms = 59 Am^2kg^{-1}; Mrs/Ms = 0.12; Chang et al. 2008), ranges from 0.3 to 6000 ppm.

Before analysis with conventional methods, the samples were observed by optical stereomicroscopy (Figure 4). On samples e4 and e14 black particles appear in the fibres. On samples e20 and h20 golden edgings are observed along the fibres suggesting the presence of pyrite. Corresponding ESEM micrographs are presented in Figure 5. On all of them bright

crystals are observed among the fibres. Sample e4 contains small crystals disseminated in the wood. Some of them present a radiative growth, typical of marcasite (White et al. 1991). On samples e14, e20 and h20 particles correspond to the agglomeration of micrometric or submicrometric crystals. A few clusters are observable on sample e14. Towards the most magnetic area, well-formed framboidal pyrite spheres appear. They are observable with a very high density around the ghost nail (e20, h20). EDS analysis confirmed that these crystals were mainly composed of sulfur and iron with an average Fe/S atomic ratio equal to 0.51 ± 0.04. This ratio corresponds to a FeS_2 stoichiometry, matching pyrite and marcasite.

Raman spectra (Figure 6) and XRD patterns (Figure 7) confirm the presence of pyrite (Raman bands at 344, 380 and 430 cm^{-1}) and marcasite (Raman bands at 323 and 386 cm^{-1}). Marcasite was mainly detected on sample e4 and e5 while pyrite was predominant in all others. Needle-like crystals composed of sulfur, oxygen and calcium were sometimes observed (Figure 8). These correspond to gypsum ($CaSO_4.2H_2O$) also detected by μ-RS (main Raman band at 1015 cm^{-1}) and XRD. The large bands at 18.7° and 26.7° or 32.6° on the diffraction patterns (Figure 7) were attributed to wood. In the most magnetic zone, namely samples e20, f20, g20 and h20, greigite (Fe_3S_4) was detected with the corresponding Raman bands at 138, 188, 250, 350 and 365 cm^{-1}. Lastly siderite ($FeCO_3$) was identified in samples g20 and h20 (Raman bands at 185, 283, 715 and 1085 cm^{-1}). This non-sulfur containing compound is often present in the rust layers of iron objects corroding in anoxic soils. This supports the close proximity of the ghost nail in these samples.

Finally, pH measurements are reported in Table 2 and show that the wood was only slightly acidic further away from the magnetic zone, with values of 5.6 for sample e4. However the pH becomes more acidic closer to the magnetic zone with values around 3. The most acidic value, at 2.6, corresponds to sample g20 containing the ghost nail. The most acidic zone around the ghost nail corresponds to the rich-pyrite zone, while the less acidic zone is richer in marcasite with respect to pyrite.

Analysis of sample g20

Sample g20 contained the ghost nail, which was extracted and analysed. It can be seen on Figure 9 that there is no residual metal remaining. The nail was completely mineralised into pyrite and siderite. A small peak at 991 cm^{-1} was observed on one Raman spectrum (Figure 9). It is typical of the SO_4^{2-} chemical group and could correspond to rozenite ($FeSO_4.4H_2O$). Magnetic analysis of both bulk sample and nail revealed the presence of greigite only with similar curves. This confirmed the absence of metal. Greigite could have been present in the wood, which remained snagged on the nail after extraction. The wood also contained a very large amount of framboidal pyrite (Figure 10). At last goethite and lepidocrocite were detected in small amounts. Their association with mineral sulfur (α-S_8) suggests an aerial oxidation of metastable iron sulfides (Figure 1).

Discussion

The magnetic measurements performed on *vaigre 11* demonstrated that the magnetic signal was due exclusively to greigite. It was assumed that it was the same throughout the entire wreck. More importantly, the presence of greigite was revealed by magnetic characterisation methods in areas where conventional techniques could not detect this mineral. The detection limit of magnetic characterisation methods is very low (below ppm) and can analyse samples in the bulk material, while XRD, ESEM or Raman spectroscopy only analyse the surface. So the

potential of such methods is particularly interesting to consider and integrate into a methodological approach aiming to exhaustively analyse the mineral phases present inside organic matter. Magnetic signals from pyrrhotite or smythite were not confirmed. We consider that they are not present in *vaigre 11*. Moreover, it was deduced by non-destructive magnetic measurements and confirmed by conventional methods that the ghost nail contained no residual metal.

Pyrite was the predominant iron-sulfur containing compound found inside the wood, either euhedral or framboidal. The framboidal form was rather concentrated around the ghost nail. Marcasite was also detected but in areas where there was a little pyrite, namely far from the ghost nail. The presence of marcasite is difficult to explain, as its mode of production is not completely understood. However in a system incorporating organic matter, anoxic conditions, water and iron, it seems relevant to assert that these iron sulfides have a bacterial origin.

The results obtained from *vaigre 11* are very different from those obtained in another study by Rémazeilles et al (2013), where mackinawite and greigite were detected, instead of pyrite. In this particular study most of the samples had been extracted from XIXth century wrecks (*USS Monitor* and wrecks of La Natière) so were considerably more recent than the wreck of Narbonne. The difference in identified iron sulfides could be explained by an effect of time, illustrated in Figure 1.

In anoxic environments, sulfide species produced by anaerobic sulfides generating bacteria precipitate with iron (II) ions produced during the corrosion of iron objects, forming mackinawite in the first instance. This mineral was able to persist for two centuries, as observed in the XIXth century wrecks. Where there is a persistent supply of sulfides, mackinawite (1 iron atom for 1 sulfur atom) is transformed into greigite (1 iron atom for 1.3 sulfur atoms) and then greigite into pyrite (1 iron atom for 2 sulfur atoms). This mechanism assimilates sulfides into the solid phases, so sulphide levels in the aqueous environment do not reach levels that impede the development of sulfides generating bacteria colonies. Consequently, the large amounts of pyrite in the wreck of Narbonne may have resulted from long-term bacterial activity and transformation of mackinawite, which was supposed to be formed in the early stages of the burial, to greigite as the intermediate product. Actually greigite can occur as an intermediate phase (i) in the transformation process of mackinawite into pyrite in anoxic environment and (ii) during the aerial oxidation of mackinawite. In its way, greigite is likely to be present under many circumstances on an “archaeological time scale” and thus can be considered as a relevant marker of iron sulfide contamination of wet archaeological wood, easily and non-destructively detectable by magnetic measurements.

Conclusion

The wood from the Mandirac wreck was abnormally magnetic. The analysis of a plank revealed a predominance of pyrite. This phase presented as framboids around a ghost nail. The nail was completely corroded into a mixture of pyrite and siderite. Greigite was detected in significant amounts and proved to be the only phase responsible for the magnetic properties of the plank and so of the wood of the entire wreck. The simultaneous presence of greigite and pyrite is in agreement with mechanisms of pyrite formation proposed in the literature and is consistent with a long-term microbiologically influenced process. In addition, the combination of conventional analytical techniques and magnetic characterisation methods was very effective in determining the mineral composition of the samples. Magnetic methods are now much more sensitive and were able to detect greigite concentrations below ppm levels. These could be used as non-

destructive diagnostic techniques for determining the presence of iron sulfides in wet archaeological materials, through the detection of greigite.

References

Bourdoiseau, J.-A., , M. Jeannin, R. Sabot, C. Rémazeilles, and Ph. Refait. 2008. Characterisation of mackinawite by Raman spectroscopy: Effects of crystallisation, drying and oxidation. *Corrosion Science* 50: 3247–3255.

Bourdoiseau, J.-A., M. Jeannin, C. Rémazeilles, R. Sabot, and Ph. Refait. 2011. The transformation of mackinawite into greigite studied by Raman spectroscopy. *Journal of Raman Spectroscopy* 42: 496-504.

Chang, L., A. P. Roberts, Y. Tang, B. D. Rainford, A. R. Muxworthy and Q. Chen. 2008. Fundamental magnetic parameters from pure synthetic greigite (Fe_3S_4). *Journal of Geophysical Research* 113(B6): 1-16.

Davis, C.W. 1935. Magnetic properties and orientation of ferromagnetic particles II. Pyrrhotite. *Journal of Applied Physics* 6: 376-379.

Dekkers, M. J., H. F. Passier, and M. A. A. Schoonen. 2000. Magnetic properties of hydrothermally synthesized greigite (Fe_3S_4) II. High- and low-temperature characteristics. *Geophysical Journal International* 141: 809–819.

Edwards, K. J., M. O. Schrenk, R. Hamers, and J. F. Banfield. 1998. Microbial oxidation of pyrite: Experiments using microorganisms from an extreme acidic environment. *American Mineralogist* 83: 1444-1453.

Fors, Y, and M. Sandström. 2006. Sulfur and iron in shipwrecks cause conservation concerns. *Chemical Society Reviews* 35: 399-415.

Garrels, R. M., and M.E. Thompson. 1960. Oxidation of pyrite by iron sulfate solutions. *American Journal of Science* 258-A: 57-67

Hoffmann, V., H. Stanjek, and E. Murad. 1993. Mineralogical, magnetic and Mössbauer data of smythite (Fe_9S_{II}). *Studia Geophysica et Geodaetica* 37: 366-381.

Hunger, S., and L. G. Benning. 2007. Greigite: a true intermediate on the polysulfide pathway to pyrite. *Geochemical Transactions* 8(1): doi:10.1186/1467-4866-8-1.

Sandström, M, F. Jalilehvand, I. Persson, U. Gelius, P. Frank, and I. Hall-Roth. 2002. Deterioration of the seventeenth-century warship Vasa by internal formation of sulphuric acid. *Nature* 415: 893–897.

Rémazeilles, C, K. Tran, E. Guilminot, E. Conforto, and P. Refait. 2013. Study of Fe (II) sulphides in waterlogged archaeological wood. *Studies in Conservation* 58(4): 297-307.

Rickard, D. and G.W. Luther. 1997. Kinetics of pyrite formation by the H_2S oxidation of iron (II) monosulfide in aqueous solutions between 25 and 125°C: The mechanism. *Geochimica et Cosmochimica Acta* 61(1): 135-147.

Roberts, A. P., L. Chang, C. J. Rowan, C.S. Horng and F. Florindo. 2011. Magnetic properties of sedimentary greigite (Fe_3S_4): an update. *Reviews of Geophysics* 49(RG1002):1-46.

Sanchez, C., and M.-P. Jézégou . 2014. Les ports antiques de Narbonne. *Les carnets du parc*. 15: 100.

Stumm, W. and J. J. Morgan. 1981. *Aquatic chemistry: An introduction emphasizing chemical equilibria in natural waters*, New York: Wiley-Interscience, p. 780.

Sullivan P. J., K.J. Reddy, and J . L . Yelton. 1988. Iron sulfide oxidation and the chemistry of acid generation. *Environmental Geological Water Science* 11(3): 289-295.

White, G. N., J.B. Dixon, R. M. Weaver and A. C. Kunkle. 1991. *Clays and Clay Minerals* 39(1): 70-76.

Wilkin, R. T. and H. L. Barnes. 1997. Formation processes of framboidal pyrite. *Geochimica et Cosmochimica Acta* 61: 323-339.

Figures captions:

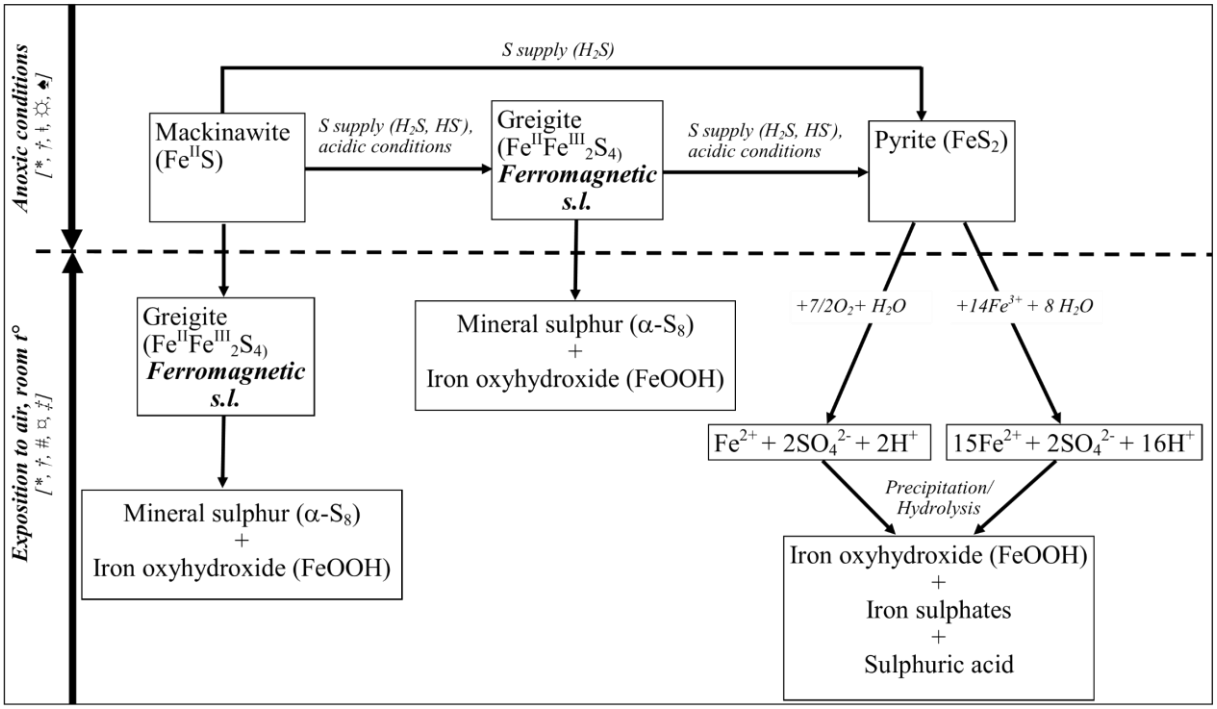

Figure 1. Diagram of the evolution and oxidation processes of mackinawite (* = Hunger and Benning 2007, † = Bourdoiseau et al. 2008, ǂ = Bourdoiseau et al. 2011, ☼ = Rickard and Luther 1997, ♠ = Wilkin and Barnes 1997, # = Garrels and Thompson 1960, ¤ = Stumm and Morgan 1981, ‡ = Sullivan et al. 1988)

Figure 2. The wreck of Mandirac (IVth century), ancient ports of Narbonne (http://pan.hypotheses.org/)

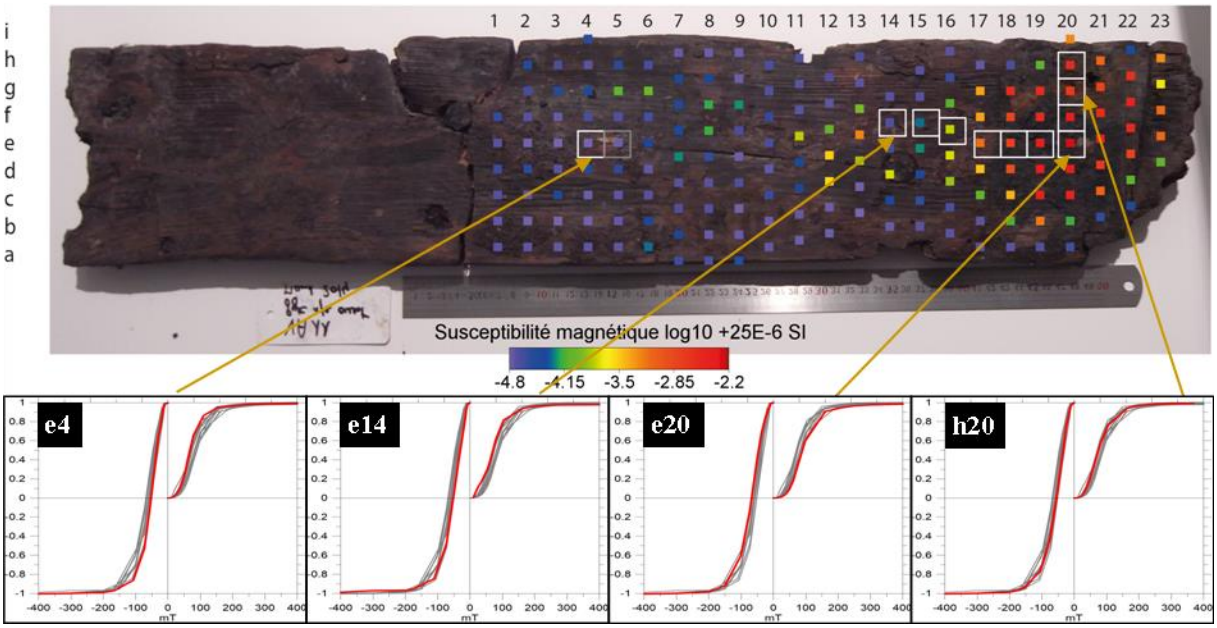

Figure 3. *Vaigre 11* with superimposed magnetic susceptibility mapping (the squares correspond to completely analysed samples) and magnetic remanence curves of e4, e14, e20 and h20 samples

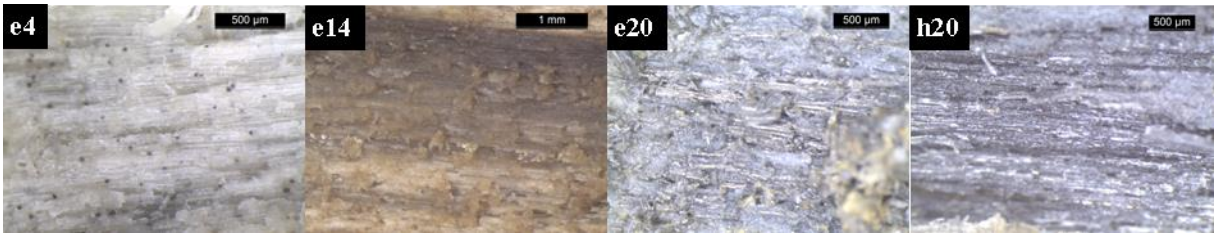

Figure 4. Pictures of wood slices cut from e4, e14, e20 and h20 samples

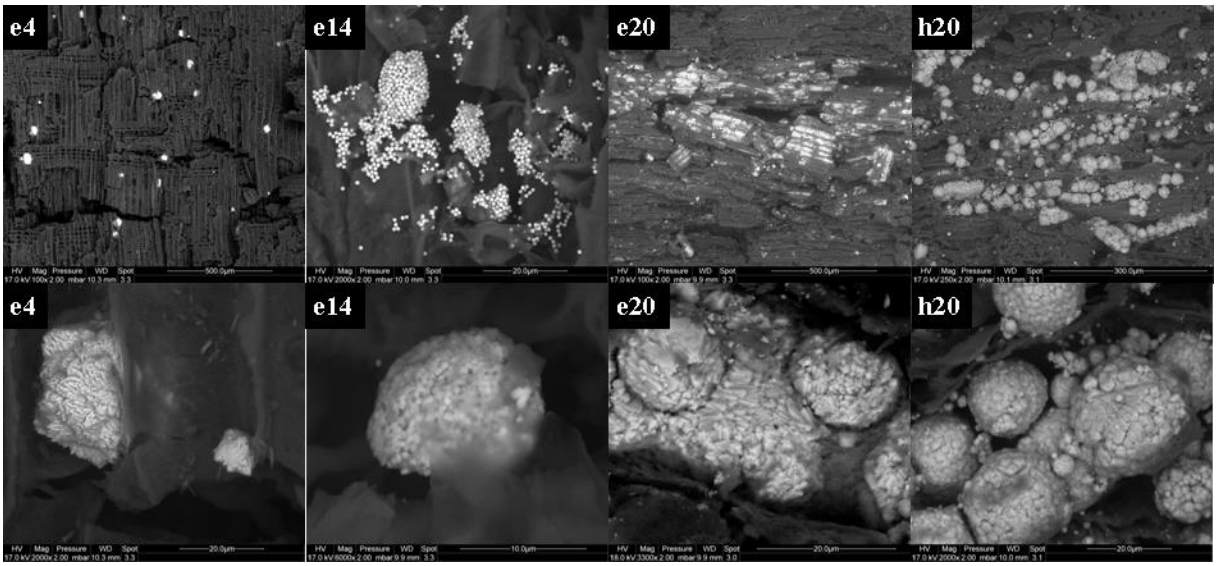

Figure 5. ESEM micrographs of e4, e14, e20, h20 samples

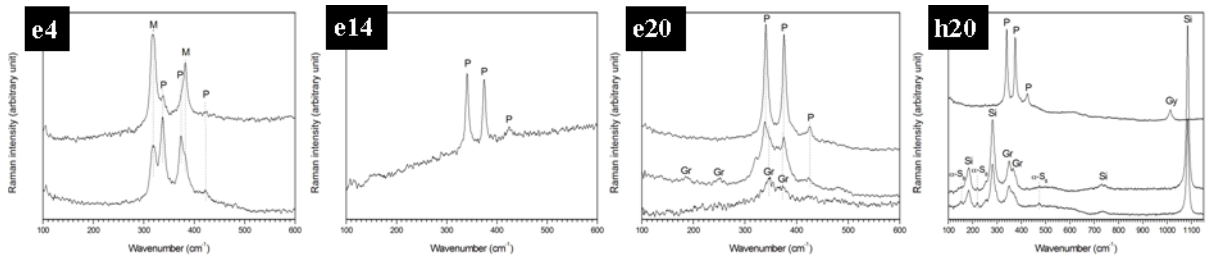

Figure 6. Raman spectra of e4, e14, e20, h20 samples (M=marcasite, P=pyrite, Gy=gypsum, Gr=greigite, Si=siderite)

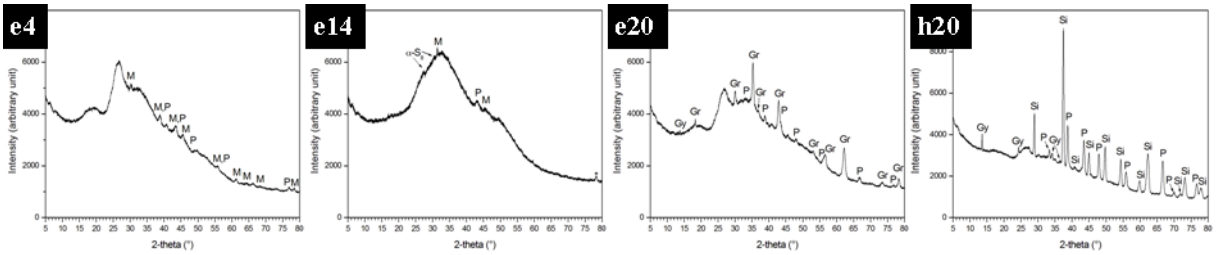

Figure 7. Diffraction patterns of e4, e14, e20, h20 samples (M=marcasite, P=pyrite, Gy=gypsum, Gr=greigite, Si=siderite, the star corresponds to the signal of the sample holder sometimes visible)

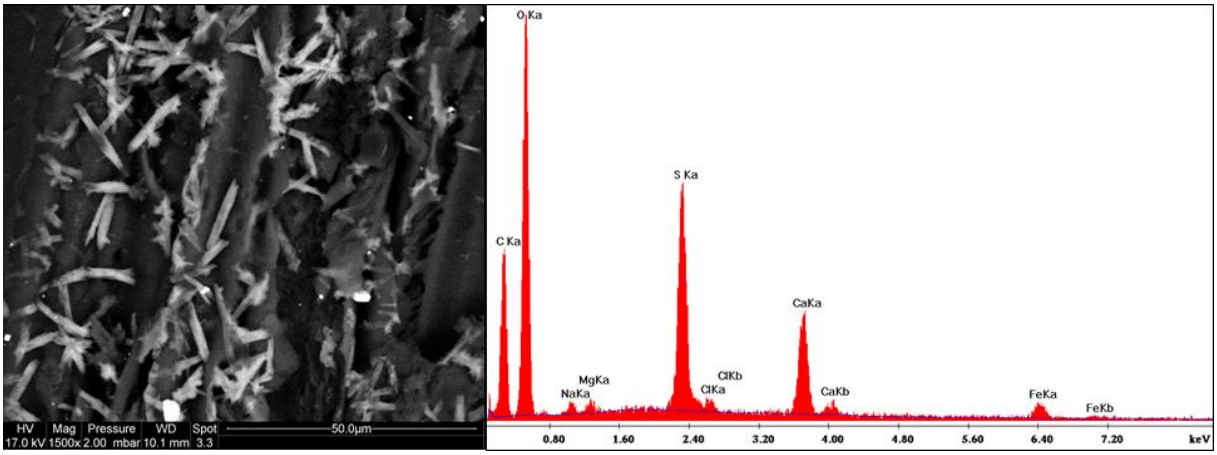

Figure 8. ESEM micrograph and EDS spectrum of gypsum detected in sample e15

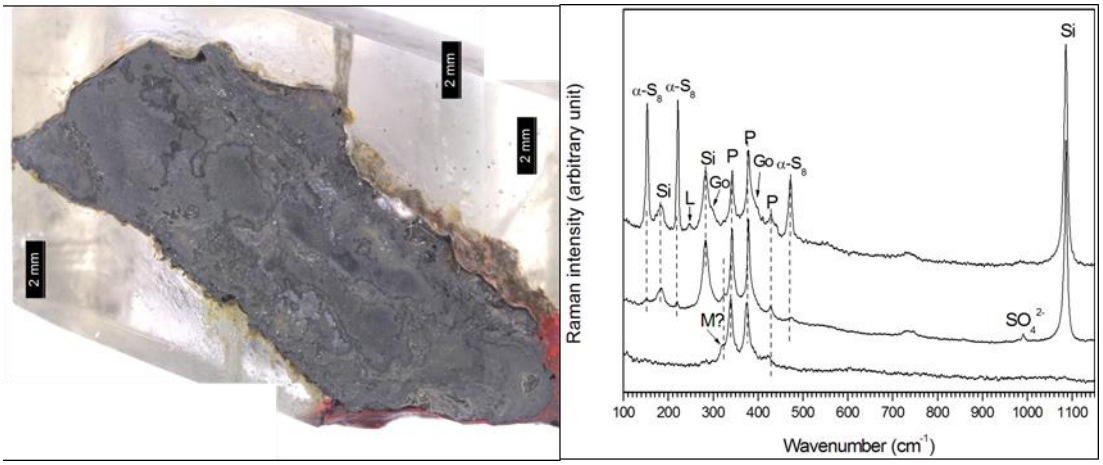

Figure 9. Picture and Raman spectra of the ghost nail extracted from sample g20 (P=pyrite, Si=siderite, Go=goethite, L=lepidocrocite, M=marcasite, α-S_8=mineral sulfur)

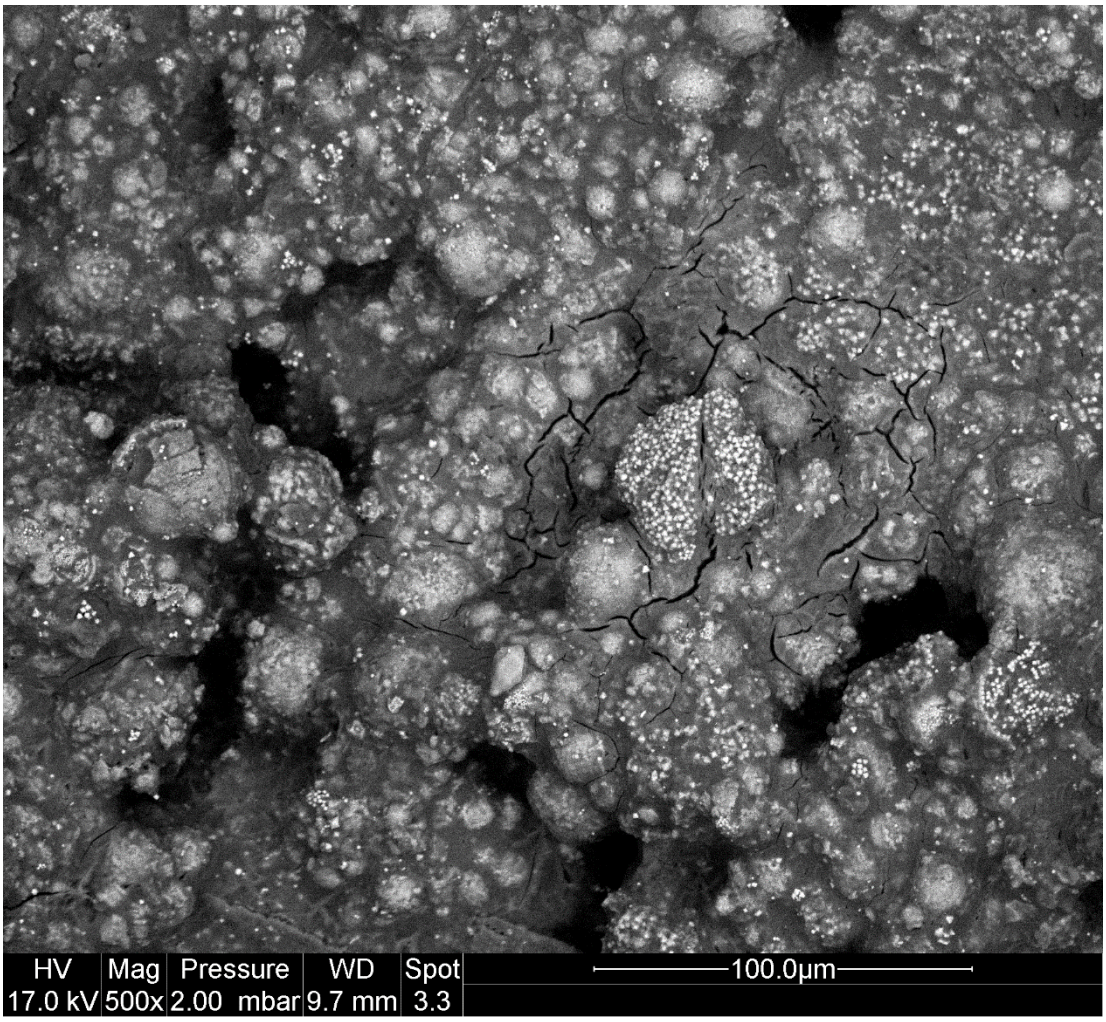

Figure 10. ESEM micrograph of the wood of sample g20

Tables captions:

Mineral	Formula	Oxidation state	Magnetic properties
Mackinawite	FeS	Fe(+II), S(-II)	Paramagnetic
Troilite	FeS	Fe(+II), S(-II)	Paramagnetic
Pyrrhotite	$Fe_{1-x}S$	Fe(+II), S(-II)	Ferromagnetic *s.l.* (Davis, 1935)
Greigite	Fe_3S_4	Fe(+II,+III), S(-II)	Ferromagnetic *s.l.* (Edwards *et al*, 1998, Dekkers *et al*, 2000)
Smythite	Fe_9S_{11}	Fe(+II,+III), S(-II) (?)	Ferromagnetic *s.l.* (Hoffmann *et al*, 1993)
Pyrite	FeS_2	Fe(+II), S_2(-II)	Paramagnetic
Marcasite	FeS_2	Fe(+II), S_2(-II)	Paramagnetic

Table 1. Naturally occurring iron (II) sulfides with oxidation states and magnetic properties

Sample	Mineral phases detected by conventional methods	Mineral phases detected by magnetic methods	pH (±0.1)
e4	Pyrite, Marcasite	Greigite	5.6
e5	Pyrite, Marcasite	Greigite	4.7
e14	Pyrite, Gypsum	Greigite	3.6
e15	Pyrite, Sulphur (α-S_8)	Greigite	4.3
e16	Pyrite, Marcasite, Gypsum, Sulphur (α-S_8)	Greigite	4.2
e17	Pyrite, Sulphur (α-S_8), Greigite	Greigite	3.5
e18	Pyrite, Sulphur (α-S_8), Greigite	Greigite	3.3
e19	Pyrite, Greigite, Gypsum	Greigite	3.3
e20	Pyrite, Greigite, Gypsum, Sulphur (α-S_8)	Greigite	3.3
f20	Pyrite, Sulphur (α-S_8), Greigite	Greigite	3.3
g20	Pyrite, Siderite ($FeCO_3$), Greigite, Sulphur (α-S_8), Rozenite ($FeSO_4.4H_2O$)	Greigite	2.6
h20	Pyrite, Siderite, Greigite, Sulphur (α-S_8), Gypsum	Greigite	2.7
i20	Pyrite, Gypsum	Greigite	*Not measured*

Table 2. Mineral composition and pH measurements of studied samples